Robotica (2016) volume 34, pp. 1495–1516. © Cambridge University Press 2014
doi:10.1017/S0263574714002616

A force-resisting balance control strategy for a walking biped robot under an unknown, continuous force

Yeoun-Jae Kim†, Joon-Yong Lee*‡ and Ju-Jang Lee§

†*Robotics Program, Korea Advanced Science and Technology, Euseong-Gu Daehak-Ro 291, Daejeon, Korea. E-mail: lethkim@kaist.ac.kr*
‡*Department of Genetics Development and Cell Biology, Iowa State University, Ames, Iowa 50011, USA*
§*Electrical Engineering, Korea Advanced Science and Technology, Euseong-Gu Daehak-Ro 291, Daejeon, Korea. E-mail: jjlee@ee.kaist.ac.kr*

(Accepted October 17, 2014. First published online: December 3, 2014)

SUMMARY
In this paper, we propose and examine a force-resisting balance control strategy for a walking biped robot under the application of a sudden unknown, continuous force. We assume that the external force is acting on the pelvis of a walking biped robot and that the external force in the z-direction is negligible compared to the external forces in the x- and y-directions. The main control strategy involves moving the zero moment point (ZMP) of the walking robot to the center of the robot's sole resisting the externally applied force. This strategy is divided into three steps. The first step is to detect an abnormal situation in which an unknown continuous force is applied by examining the position of the ZMP. The second step is to move the ZMP of the robot to the center of the sole resisting the external force. The third step is to have the biped robot convert from single support phase (SSP) to double support phase (DSP) for an increased force-resisting capability. Computer simulations and experiments of the proposed methods are performed to benchmark the suggested control strategy.

KEYWORDS: Biped robot; Inverted pendulum model; Balance control; Continuous force.

1. Introduction

Until recently, a large number of papers have been published on movement control of humanoid and biped robots. A biped has two legs and is more maneuverable compared with wheeled mobile robots. When crossing small obstacles, the biped simply steps over the obstacles, while wheeled robots must go around the obstacles. However, controlling a biped robot is more difficult than a wheeled mobile robot, because of its highly-coupled, non-linear dynamics. Vukobratovic and Borovac[1] redefined the ZMP, which has been used for 35 years in biped robot control. McGeer[2] analyzed basic human motion using non-linear dynamics.

Walking, jumping and running motions of biped robots have been major topics of research because they are the basic types of motion for a biped robot. Geng and Gan[3] designed a planar biped walking gait using state machines. Berenguer and Monasterio-Huelin[4] designed a walking robot called "Zappa", which is a biped robot with a tail. Sato *et al.*[5] designed a real-time walking trajectory for a biped robot using the three mass model. Goswami and Vadakkepat[6] designed planar bipedal jumping gaits with stable landing. Kajita *et al.*[7] designed a biped capable of running by using the ZMP-based control method. These studies represent only a small number of the numerous studies investigating the basic movability of a biped robot.

* Corresponding author. E-mail: junyoni@gmail.com

A number of questions exist concerning the stability of a biped robot under an externally applied force. First, the push recovery strategies of a standing biped robot are currently being examined. There are three types of strategies. The "ankle strategy", the "hip strategy" and the "step out strategy". The ankle and hip strategies involve a small or intermediate externally applied force that the robot can withstand using ankle and hip torque control. Huang *et al.*[8] suggested an ankle angle compensation strategy against a small external disturbance. The feedback linearizing control of a simple double-inverted pendulum model using ankle and hip torque was investigated by Hemani and Camana[9]. The hip strategy described by Horak and Nashner[10] was a mainframe description of the hip balance control strategy. Nenchev and Nishio[11] suggested ankle and hip strategies for the balance recovery of a biped that is subjected to an impact. Stephens[12] used the two-link model and integral (ankle plus hip) strategies to balance a standing robot. The step out strategy is used when an external disturbance force is too large and the robot cannot withstand the disturbance using ankle and hip torque control. Stepping to avoid falling was studied by Goddard *et al.*[13]. Winter[14] analyzed human balance and posture control during standing and walking. Deng-Peng and Xu[15] suggested multiple balance strategies for humanoid standing control. These three strategies were explained by Stephens.[16]

A number of research papers have described the balance control strategy of a walking biped robot that is subject to an externally applied force. These papers assumed that the force is impulsive and forces the robot to rotate suddenly with an angular velocity with respect to the stance leg. Pratt *et al.*[17] suggested a capture point to compensate for and stabilize a biped robot in a sudden angular velocity situation by using the step out strategy. Motoi *et al.*[18] suggested real-time gait planning for the pushing motion of a humanoid robot by using the inverted pendulum model. Harada *et al.*[19] designed a walking motion to manipulate the pushing motion to a humanoid robot. Komura *et al.*[20] suggested a feedback controller capable of counteracting a large perturbation in the sagittal plane. Yasin *et al.*[21] used the capture point to stabilize a walking biped robot that was subjected to an externally applied force by using the step out strategy. Yi *et al.*[22,23] used the capture point and reinforcement learning to stabilize a walking biped robot that was subject to an externally applied force. Li *et al.*[24] designed a dynamic balance control for a walking biped robot using sensor fusion, the Kalman filter and fuzzy logic.

Previous papers that focused on balancing a walking biped robot that is subject to an externally applied force assumed that the force was impulsive. However, an externally applied force can be continuous. For example, in the future, children could push a walking in-house service robot with a continuous force. In such a case, balancing the walking biped robot is an important safety issue. In this paper, we suggested a balance control strategy for a walking biped robot under an unknown, continuous external force. The suggested control strategy can be applied when an unknown external force is either continuous or impulsive. Moreover, previous papers assumed that the force is acting in the $+Y$ direction only. The suggested control strategy can also be applied when the external force is acting in the $-Y$ direction. This paper is a supplement to one of our previous papers.[25] Compared with paper [25], we included the experimental results and the simulation results of the case where an external force acts in the $-Y$ direction.

The subsequent sections are as follows. The motivation of this research is explained in Section 2. The biped model and the pre-defined walking gait trajectory for the simulations and the experiments are described in Section 3. In Section 4, the force-resisting balancing control strategy is proposed and described. In Section 5, the simulation results are illustrated and explained. In Section 6, the experimental results are explained and in Section 7, the conclusion is drawn.

2. Motivation

2.1. Implication of a continuous external force

As noted in the introduction, the balance strategy in the case of an impulsively applied external force sometimes cannot be applied directly to the case of a continuously applied external force. We will demonstrate this point by using an open dynamics engine (ODE).[26] The robot model used in this ODE simulation is given in Fig. 1. We used the capture point [17] as the balance control strategy in the ODE simulation because the capture point is the most widely used control strategy. The capture point [17] determines the step length in which the initial energy of a pushed robot disappears. If the

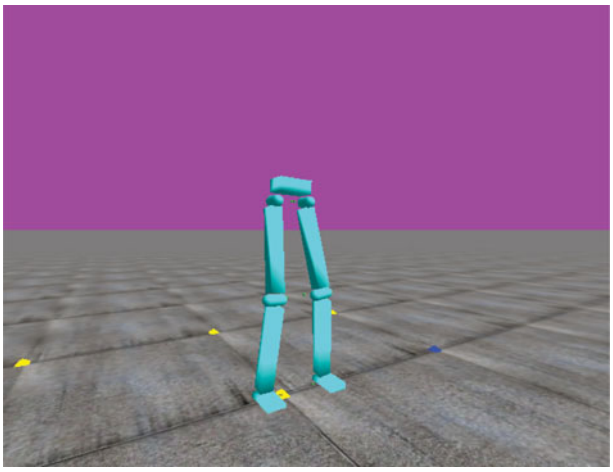

Fig. 1. The biped model in ODE simulation.

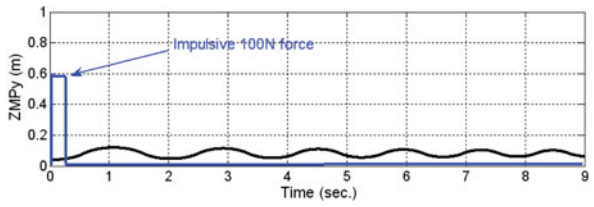

(a) Impulsive force case

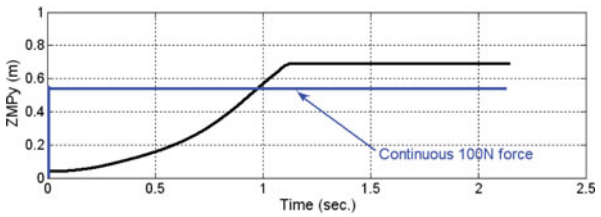

(b) Continuous force case

Fig. 2. The ODE simulation results using the capture point. (a) Impulsive force case. (b) Continuous force case.

initial energy disappears by stepping to the capture point, the robot can be stabilized. The equation governing this is described in (1).

$$
\begin{aligned}
&y_{capture} = \dot{y}\sqrt{\tfrac{z_0}{g}} \\
&y_{capture} \text{ :step length} \\
&\dot{y} \text{ :initial velocity of mass center} \\
&z_0 \text{ :height of mass center} \\
&g \text{ :acceleration of gravity.}
\end{aligned}
\tag{1}
$$

Figure 2 represents the simulation results obtained using the capture point strategy. The graph in Fig. 2(a) represents the impulsively applied force case and the graph in Fig. 2(b) represents the continuously applied force case. A force of 100 N is applied to the center of mass of the robot. The ZMP_y profile of the graph in Fig. 2(a) represents a stable oscillation, which implies that the robot did not fall down but was stabilized when subjected to an impulsively applied force of 100 N. However, the ZMP_y profile seen in the graph of Fig. 2(b) rapidly reaches the upper limit of 0.7 m, which means that the robot fell down rapidly when subjected to a continuously applied force of 100 N.

Thus, the balance control strategy used in the impulsive external force case cannot be used in the continuous external force case.

2.2. Main ideas

For a more concrete understanding of our proposed strategy, we describe the problem and the proposed solution. The problem is that when the biped is walking, an unknown and continuous force is suddenly applied to the center of the pelvis of the biped robot. If there is no control, the ZMP of the robot moves out of the sole of the biped, and the robot eventually falls down. To prevent the robot from falling down, a control strategy must be applied to the robot. We propose a force-resisting control strategy, that uses ZMP feedback. The Lagrangian formulation of the governing equation of this situation is written in (2)

$$
\begin{aligned}
&M(q)\ddot{q} + V(q,\dot{q}) + G(q) = Q \\
&Q = \tau \pm J_p^T F_e \\
&\\
&q \text{ :Joint angles of a biped robot} \\
&\dot{q} \text{ :Joint velocities of a biped robot} \\
&\ddot{q} \text{ :Joint accelerations of a biped robot} \\
&\\
&M(q) \text{ :Mass matrix} \\
&V(q,\dot{q}) \text{ :Centrifugal and Coliolis acceleration term} \\
&G(q) \text{ :Gravitational force term} \\
&Q \text{ :Overall joint torques (joint torques + external force)} \\
&\\
&\tau \text{ :Joint torques of a biped robot} \\
&J_p \text{ :Jacobian of the center of pelvis} \\
&F_e \text{ :the suddenly applied unknown and continuous external force.}
\end{aligned}
\tag{2}
$$

Because we utilize ZMP feedback control, the posture of the robot counteracts the external force when the balance control strategy is applied to the robot. This is depicted in Fig. 3 which shows the front of the biped robot and explains that when a sudden external force is applied to the walking robot, the robot counteracts the external force to prevent itself from falling by using the balance control strategy and subsequently switches from SSP to DSP for additional stability.

3. The Biped Robot and Walking Gait

We represent the biped robot and the pre-defined biped walking gait that are used in the simulations and experiments in this section. In our previous study,[27] we constructed an energy efficient biped walking trajectory by utilizing the Tchebyshev method. We use this methodology in this paper to design a pre-defined walking gait.

The biped robot used in the simulations and experiments is called "LRH-1". LRH-1 has 12 degree of freedom (DOF), where each leg has 6 DOF. The joint motors of LRH-1 are position-controllable. The schematics of LRH-1 are shown in Fig. 4. The left-hand image in Fig. 4 represents the 12 local coordinates and geometrical characteristics of LRH-1. The right-hand image in Fig. 4 represents the sole of LRH-1. The ZMP stability region in Fig. 4 will be explained in Section 4. All of the geometrical data are summarized in Table I. We modeled LRH-1 as serial links with a point mass because the exact inertia matrix is difficult to measure. The designed walking gait sequence that is used in the simulations is shown in Figs. 5 and 6. LRH-1 is viewed sagitally in Fig. 5 and laterally in Fig. 6. The left leg is set backward as the swing leg and the right leg is the stance leg. As the gait progresses from 0 s to 3.250 s, the foot of the stance leg remains stationary and the foot of the swing leg is set forward to perform a stride. The floor is a black horizontal line where the sole of the stance

Table I. Geometrical data.

Length (mm)											
L_1	L_2	L_3	L_4	L_5	L_6	L_7	L_8	L_9	L_{10}	W_1	W_2
60	99.9	48	23.5	52	71.7	60	52	42.5	80.5	42	69.9

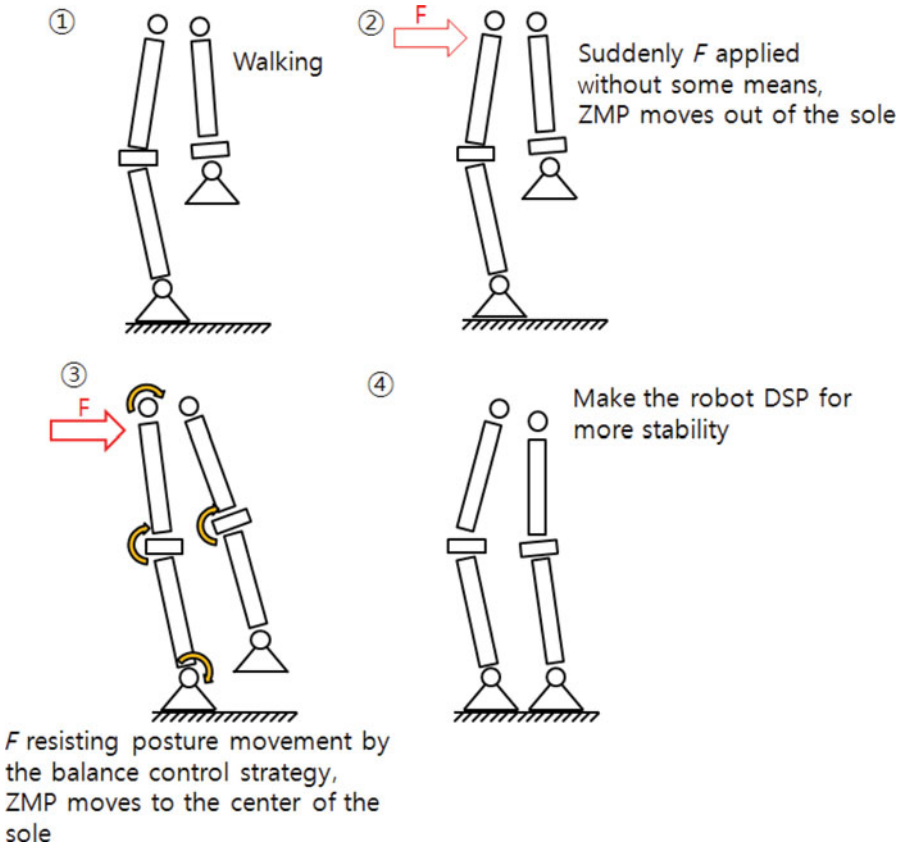

Fig. 3. The force resisting balance control of a walking biped robot.

foot lies. The overall walking time is 3.250 s, and the walking stride is approximately 0.15 m. The sampling rate in the simulations is 1 kHz.

The overall appearance of LRH-1 is shown in Fig. 7. LRH-1 was constructed with 12 RX-24F motors. The specification of the biped robot LRH-1 and the motor(RX-24F of Dynamixel Inc.) is presented in Table II. A notebook(Intel Core i5 CPU, 3.24 Gbytes of RAM) is used to control LRH-1. LRH-1 and the controlling unit are connected via the IEEE 485 protocol. The sampling rate of LRH-1 is 30 Hz. The overall walking pattern is shown in Fig. 8. Using the designed walking gait sequence, we preformed the walking experiment with LRH-1 and tuned the angle values slightly with respect to the measured ZMP value. The walking stride is approximately 0.15 m, which is the same as that of the simulation. The overall walking time is approximately 9.75 s, which is three times longer than that of the simulation. The reason for the longer walking time is because if the walking time is too short, it is difficult to continue pushing the torso of LRH-1 with a finger.

4. Proposed Force-Resisting Balance Control Strategy

In this section, the force-resisting balance control strategy is proposed and explained. The control strategy is divided into three steps. The first step is detecting the unknown, continuous external force.

Table II. The data of LRH-1 and RX-24F.

RX-24F property			LRH-1 property		
Physical property	Value	Unit	Physical property	Value	Unit
Resolution	0.33	Degree	Weight	1162	g
Stall Torque	26	kgf.m	Height	31	cm
Weight	96.83	g	DOF	12	

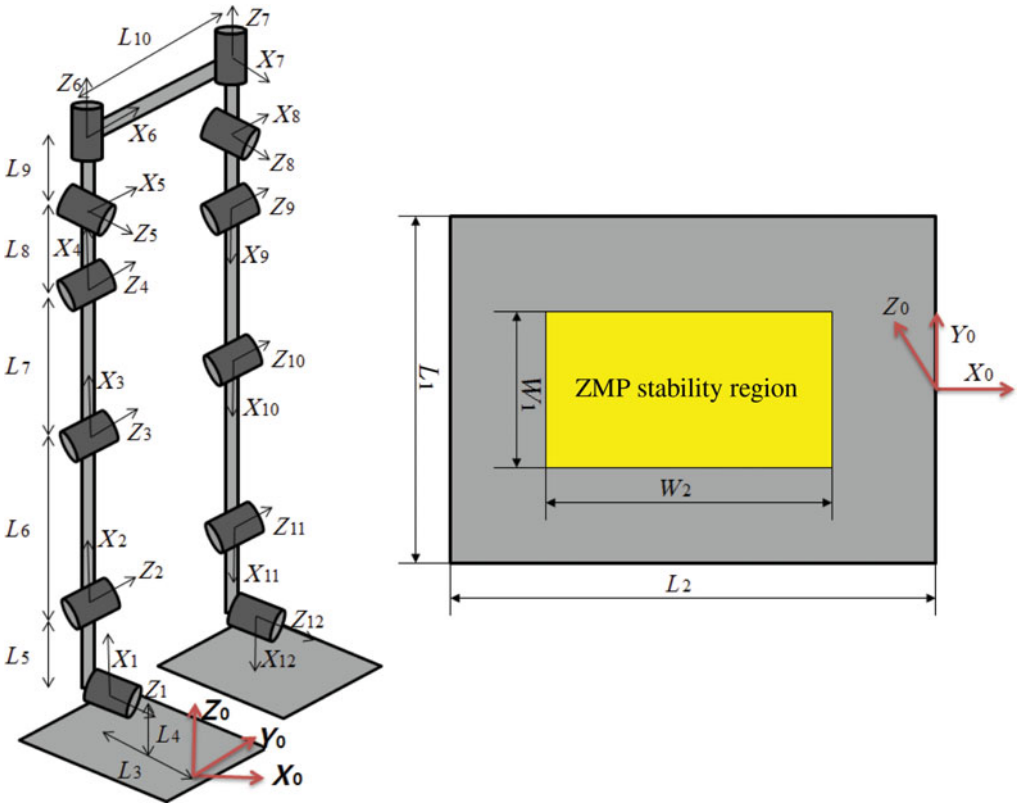

Fig. 4. LRH-1 model.

The second step is to move the ZMP of the biped robot to the center of the sole of the robot. The third step is for the biped robot to transition from the SSP to the DSP for additional stability. The subsections explain these three steps.

4.1. STEP 1: Detecting the abnormal situation

In this subsection, we explain how the abnormal situation is detected by the biped robot. We use only the ZMP information of the biped robot. No other sensor implementation is needed. An abnormal situation is a situation in which an unknown, continuous external force is applied to the robot. We define the ZMP stability boundary, which is described in Fig. 4. The region of the right picture in Fig. 4 is the sole of the robot. Its size is 60 mm $\times$ 99.9 mm. The stability region is a 42 mm $\times$ 69.9 mm green rectangle that is located at the center of the sole. The ZMP of the walking robot is located within the ZMP stability region because we constructed the pre-defined gait in such a manner. Therefore, if the ZMP is in the stability region, the robot senses that nothing has happened. However, if the ZMP departs from the ZMP stability region, the robot senses an external force is being applied.

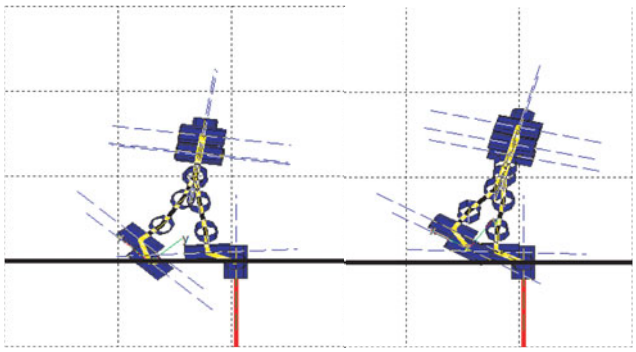

(a) 0 sec (b) 0.812 sec

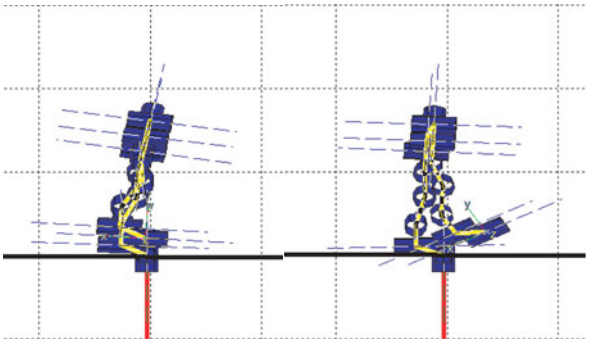

(c) 1.625 sec (d) 2.437 sec

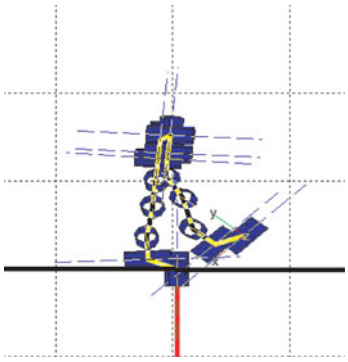

(e) 3.250 sec

Fig. 5. Walking gait sequence of LRH-1 model (in sagittal view). (a) 0 s. (b) 0.812 s. (c) 1.625 s. (d) 2.437 s. (e) 3.250 s.

4.2. STEP 2: Moving the ZMP to the center of the sole

The next step is to move the ZMP to the center of the sole of the robot. First, the controller converts the ΔZMP to ΔCOG(Δ Center Of Gravity) based on Eqs. (3) and (4). This is the inverted pendulum model[28] expanded using a discrete finite time difference.

$$\Delta ZMP = \Delta COG - \frac{Zc}{g} C\ddot{O}G \times \delta t^2$$

Zc :the height of COG of the biped robot

g :the gravitational acceleration

$C\ddot{O}G$:2nd time derivative of COG

δt :time increment(0.001 s) (3)

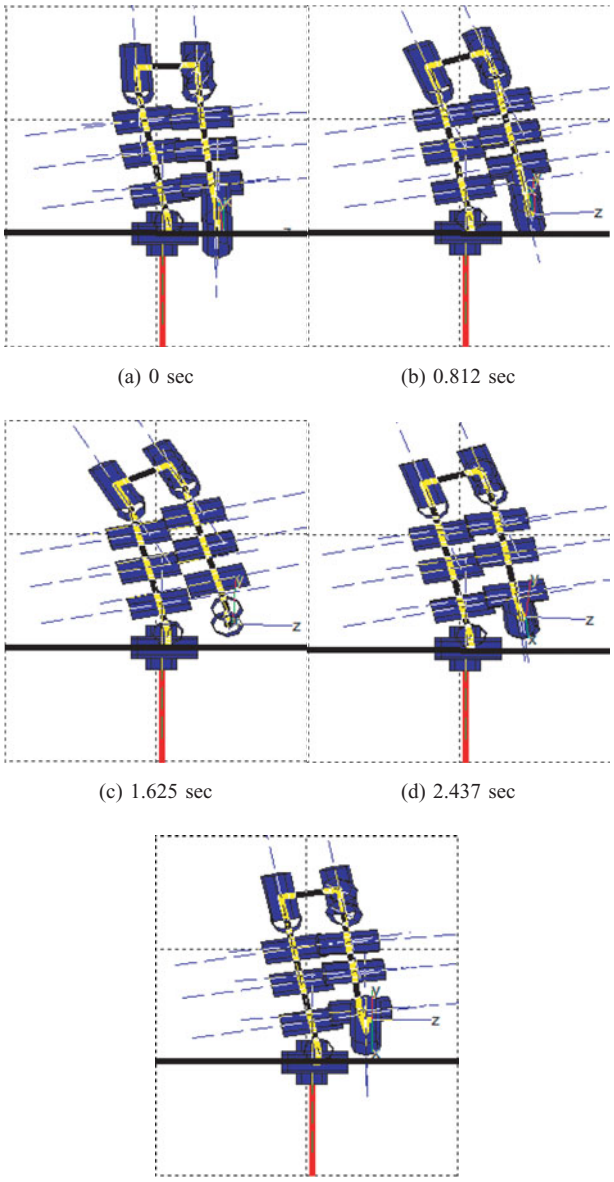

(a) 0 sec (b) 0.812 sec

(c) 1.625 sec (d) 2.437 sec

(e) 3.250 sec

Fig. 6. Walking gait sequence of LRH-1 model (in lateral view). (a) 0 s. (b) 0.812 s. (c) 1.625 s. (d) 2.437 s.

$$\begin{gathered}\Delta COG = \Delta ZMP + \frac{Zc}{g}\times \\ \{2COG(t-1) - 5COG(t-2) \\ +4COG(t-3) - COG(t-4)\} \\ COG(t-1) \text{ :COG at t-1 time(one step before time t)} \\ COG(t-2) \text{ :COG at t-2 time(two steps before time t)} \\ COG(t-3) \text{ :COG at t-3 time(three steps before time t)} \\ COG(t-4) \text{ :COG at t-4 time(four steps before time t).}\end{gathered} \tag{4}$$

The ΔZMP is the target ZMP minus the current ZMP. We make this increment 0.01 mm in the Y direction. The sampling frequency is 1 kHz. in the simulation as explained in Section 3. With this

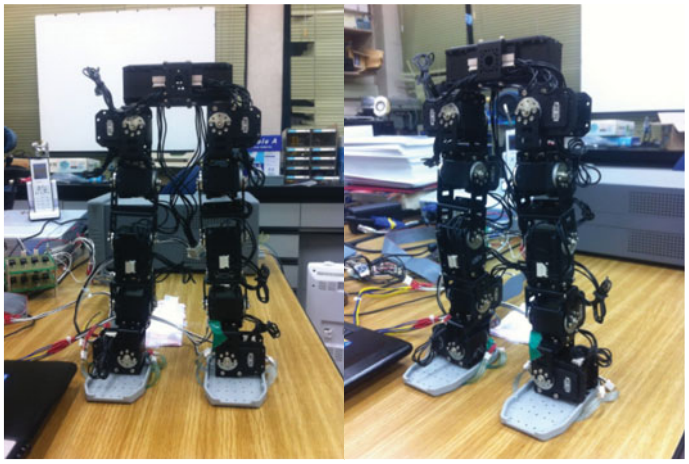

(a) Front view (b) Side view

Fig. 7. Overall appearance of biped robot LRH-1. (a) Front view. (b) Side view.

sampling frequency, if ΔZMP is large, ΔCOG will also be large which makes the COG Jacobian constraint error large. Using a safety factor, we set this increment value to 0.01 mm. After calculating ΔCOG, we calculate $\Delta\hat{\theta}_t$, the motor angle increments by the COG Jacobian and constrained linear quadratic programming. The COG Jacobian and constrained linear quadratic programming in robot balance were first introduced by Sugihara and Nakamura.[29] The detailed equations are below:

$$\hat{\theta}_t = \begin{bmatrix} \theta_1 & \theta_2 & \theta_3 & \theta_4 & \theta_5 & \theta_6 & \theta_7 & \theta_8 & \theta_9 & \theta_{10} & \theta_{11} & \theta_{12} \end{bmatrix}_t^T$$

$\hat{\theta}_{t\,\mathrm{arg}\,et}$: Target $\hat{\theta}$

$$\Delta^{cmd}\hat{\theta}_t = (\hat{\theta}_{t\,\mathrm{arg}\,et} - \hat{\theta}_{t-1})$$

$$\Delta\hat{\theta}_t = (\hat{\theta}_t - \hat{\theta}_{t-1})$$

$$\text{Minimize } \frac{1}{2}(\Delta^{cmd}\hat{\theta}_t - \Delta\hat{\theta}_t)^T W(\Delta^{cmd}\hat{\theta}_t - \Delta\hat{\theta}_t)$$

$$\text{Subject to } J_{COG}\Delta\hat{\theta}_t = \Delta COG$$

$$-0.01^\circ < \Delta\hat{\theta}_t < +0.01^\circ$$

$$J_{COG} = \begin{bmatrix} \frac{\partial COG_x}{\partial\theta_1} & \frac{\partial COG_x}{\partial\theta_2} & \cdots & \frac{\partial COG_x}{\partial\theta_{12}} \\ \frac{\partial COG_y}{\partial\theta_1} & \frac{\partial COG_y}{\partial\theta_2} & \cdots & \frac{\partial COG_y}{\partial\theta_{12}} \\ \frac{\partial COG_z}{\partial\theta_1} & \frac{\partial COG_z}{\partial\theta_2} & \cdots & \frac{\partial COG_z}{\partial\theta_{12}} \end{bmatrix} \tag{5}$$

COG_x : x coordinate of COG

COG_y : y coordinate of COG

COG_z : z coordinate of COG

$$\mathrm{W} = \begin{bmatrix} 1 & 0 & \cdots & 0 \\ 0 & 1 & \cdots & 0 \\ \vdots & \vdots & \ddots & \vdots \\ 0 & 0 & \cdots & 500 \end{bmatrix},$$

$\hat{\theta}_t$ in Eq. (5) is the 12 joint motor angles, which must be calculated and activated at time t. $\hat{\theta}_{target}$ in Eq. (5) is the 12 target motor angles. The target motor angles are determined using the inverse kinematics in which the robot is in DSP with minimal angular displacement from the biped posture at

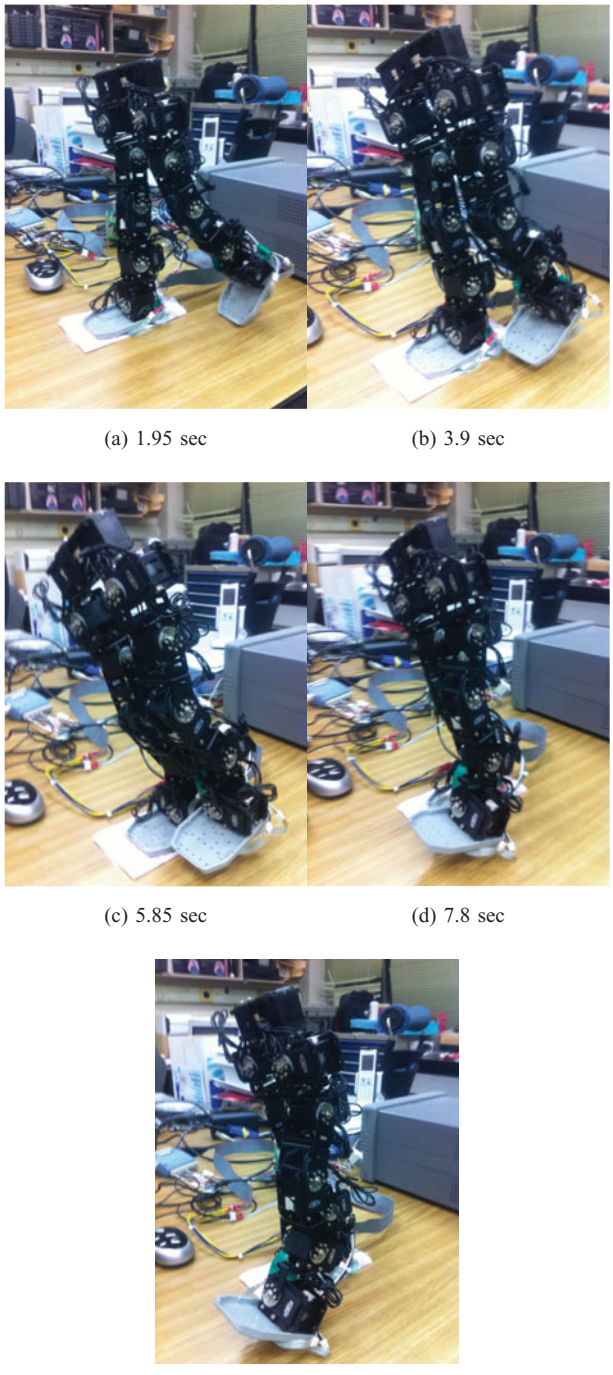

(a) 1.95 sec (b) 3.9 sec

(c) 5.85 sec (d) 7.8 sec

(e) 9.75 sec

Fig. 8. Walking pattern of LRH-1. (a) 1.95 s. (b) 3.9 s. (c) 5.85 s. (d) 7.8 s. (e) 9.75 s.

which the abnormal situation happened. The object function in Eq. (5) is for minimizing the distance between $\Delta^{cmd}\hat{\theta}_t$ and $\Delta\hat{\theta}_t$ using two constraints. W is the weighting matrix in (5). All the diagonal elements of the weight matrix are 1 except for the 5 elements in the lower diagonal which are set to 500 because the left leg must track the target angle more rigorously. This value(500) is deduced by trial and error by incrementing the element to 10, 50, 100, 500, 1000, 5000 and 10,000, and we determined that 500 is the optimal value. For the constraints, the values of the upper and the lower range of $\Delta\hat{\theta}_t$ are set to $+0.01^\circ$ and -0.01°, respectively. This is because the solution must be in this range to finely control the actuating motors. The COG Jacobian is another constraint that must be

satisfied. The definition of the COG Jacobian is J_{COG} in Eq. (5). In short, the ZMP control logic determines ΔZMP and calculates ΔCOG and $\Delta\hat{\theta}_t$ using the linear quadratic constrained optimization technique.

4.3. STEP 3: Make the robot DSP

Step 3 is to make the robot switch from the single support phase to the double support phase for additional stability against the external force. The gait control logic is divided into three consequent actions.

- If the swing leg is at a higher position, move the swing leg to a lower position by using the foot-tip Jacobian-based constrained optimization.
- Stretch the swing leg.
- Contract the stance leg.

The following equation is used to swing the leg to a lower position by using the foot-tip Jacobian-based constrained optimization:

$$\hat{\theta}_t = \begin{bmatrix} \theta_1 & \theta_2 & \theta_3 & \theta_4 & \theta_5 & \theta_6 & \theta_7 & \theta_8 & \theta_9 & \theta_{10} & \theta_{11} & \theta_{12} \end{bmatrix}_t^T$$

$\hat{\theta}_{t\,\mathrm{arg}\,et}$: Target $\hat{\theta}$

$$\Delta^{cmd}\hat{\theta}_t = (\hat{\theta}_{t\,\mathrm{arg}\,et} - \hat{\theta}_{t-1})$$

$$\Delta\hat{\theta}_t = (\hat{\theta}_t - \hat{\theta}_{t-1})$$

$$\text{Minimize } \frac{1}{2}(\Delta^{cmd}\hat{\theta}_t - \Delta\hat{\theta}_t)^T W(\Delta^{cmd}\hat{\theta}_t - \Delta\hat{\theta}_t)$$

$$\text{Subject to } J_{foottip}\Delta\hat{\theta}_t = \Delta foottip$$

$$-0.00^\circ < \Delta\theta_1 \cdots \Delta\theta_6 < +0.00^\circ$$

$$-0.01^\circ < \Delta\theta_7 \cdots \Delta\theta_{12} < +0.01^\circ$$

$$J_{COG} = \begin{bmatrix} \frac{\partial foottip_x}{\partial\theta_1} & \frac{\partial foottip_x}{\partial\theta_2} & \cdots & \frac{\partial foottip_x}{\partial\theta_{12}} \\ \frac{\partial foottip_y}{\partial\theta_1} & \frac{\partial foottip_y}{\partial\theta_2} & \cdots & \frac{\partial foottip_y}{\partial\theta_{12}} \\ \frac{\partial foottip_z}{\partial\theta_1} & \frac{\partial foottip_z}{\partial\theta_2} & \cdots & \frac{\partial foottip_z}{\partial\theta_{12}} \end{bmatrix} \tag{6}$$

$foottip_x$: x coordinate of $foottip$

$foottip_y$: y coordinate of $foottip$

$foottip_z$: z coordinate of $foottip$

$$\mathrm{W} = \begin{bmatrix} 1 & 0 & \cdots & 0 \\ 0 & 1 & \cdots & 0 \\ \vdots & \vdots & \ddots & \vdots \\ 0 & 0 & \cdots & 1 \end{bmatrix}.$$

The variables and object function of Eq. (6) are the same as that of Eq. (5). In this case, the weight matrix W in the object function is the identity matrix as shown in Eq. (6). The constraints make use of the foot-tip Jacobian. The foot-tip is the foot-tip of the swing leg(left leg). Δfoot-tip is the amount of the foot-tip displacement in which the controller attempts to move the foot-tip of the biped robot. In the simulation, Δfoot-tip was entered as the increment value with which we want to lower the left leg. The actual value is −0.1 mm in the Z direction. The $\Delta\theta_n$ constraints in Eq. (6) show that only $\Delta\theta_7 \sim \Delta\theta_{13}$ are valid optimization parameters. All others are simply dummy(zero) parameters. This is because only the left leg(the swing leg) must be moved to a lower swing leg position. After lowering the swing leg, stretching the swing leg and contracting the stance leg using inverse kinematics shifts the robot from the single support phase to the double support phase. It was assumed that during Step 3, the external force acts on the COG of the robot, but the leverage effect caused by the external force

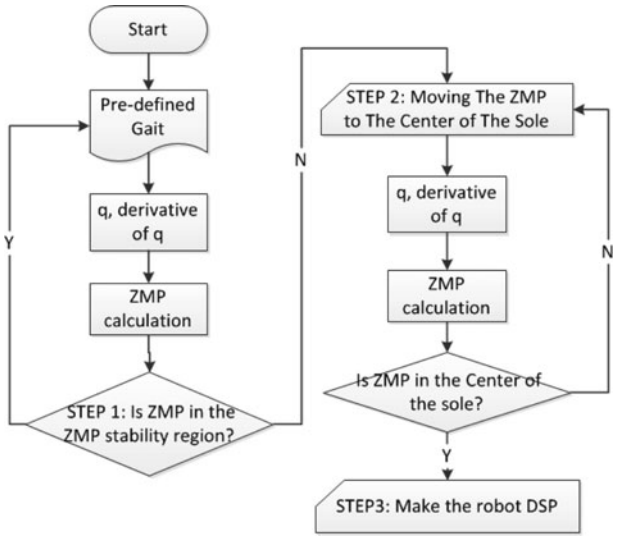

Fig. 9. Overall balance control schematics.

cannot occur, and the external force just slightly moves the ZMP. Actually, for the leverage effect to occur, the ZMP must be out of the sole region, however, contracting the stance leg actually moves the ZMP slightly. The overall control strategy is depicted in Fig. 9.

5. The Simulation Results

The computer simulation results are explained in this section. The simulations were performed in conjunction with the pre-defined gait simulation. The sampling frequency was 1 kHz, as explained previously. When calculating the time derivative of the angular displacement of the motors, the backward finite difference formula(error: $O(h^2)$) is used. We calculated the ZMP using the Newton-Euler formation by using the equation below:

$$ZMP = \frac{Z_0 \times M_0}{Z_0 \cdot F_0}. \tag{7}$$

In Eq. (7), Z_0 is the $+Z$ direction vector of origin and M_0 and F_0 are the moment and force, respectively, acting on the sole of the biped robot. The X_0, Y_0, Z_0 coordinate system is shown in Fig. 4. The simulation conditions are summarized in Table III. There are six cases in this simulation. The X direction forces are 0 N and ± 0.05 N, and the Y direction forces are +0.4 N and -1.2 N. The force is applied at a quarter of the walking duration when the -1.2 N force is applied, and at half of the walking duration when the +0.4 N force is applied. We selected force applying times and the amount of the applied force in this way because if a force of -1.2 N is applied at a quarter of the walking duration, the ZMP will depart from the ZMP stability boundary at half of the walking duration. In addition, the ZMP will depart from the ZMP stability boundary when a force of +0.4 N is applied at half of the walking duration. Using these simulation conditions, we can investigate the behavior of the proposed balance control strategy when the Step 2 phase is entered subsequent to the activation of the external force and sometime after the activation of the external force. A force of ± 0.05 N in the X-direction is the perturbation force. The simulation machine contains an Intel Core i5 CPU and 3.24Gbytes of RAM.

5.1. The gaits characteristics

The gaits in the simulation results for Cases 1, 2 and 3 are presented in Fig. 10. Cases 1, 2, and 3 represent almost identical gaits because there is only a perturbation force difference of ± 0.05 N in the X direction(these perturbation forces do not influence the gaits). Figure 10(a) and (b) are from a sagittal plane view, and Fig. 10(c) and (d) are from a lateral plane view. Figure 10(a) represents the initial posture of the biped. The left leg is set backward, and the right leg is the stance leg. The

Table III. Simulation conditions.

Applied forces (N)			Force applying time	
Case	*X* direction	*Y* direction	Case	Portion of walking time
1	0	0.4	1	
2	0.05	0.4	2	A half of walking time
3	−0.05	0.4	3	
4	0	−1.2	4	
5	0.05	−1.2	5	A quarter of walking time
6	−0.05	−1.2	6	

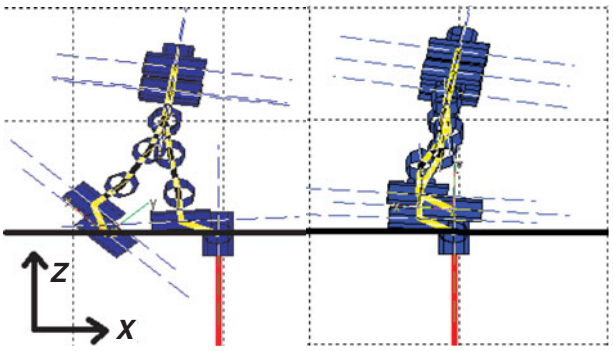

(a) Beginning (0 sec) (b) Force application starts (Step 2 starts) (1.626 sec)

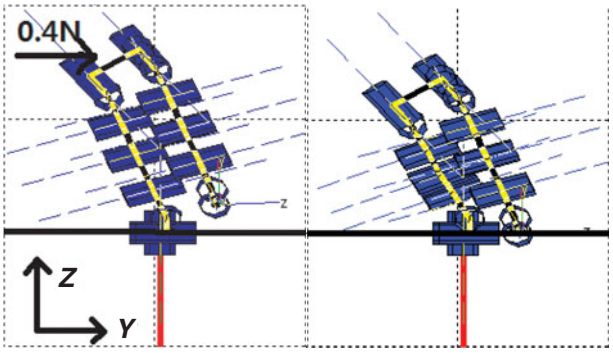

(c) Step 2 ends (Step 3 starts) (3.904 sec) (d) Step 3 ends (4.904 sec)

Fig. 10. Balancing pictures of LRH-1 (Case 1, 2, 3). (a) Beginning (0 s). (b) Force application starts (Step 2 starts) (1.626 s). (c) Step 2 ends (Step 3 starts) (3.904 s). (d) Step 3 ends (4.904 s).

external force is applied in Fig. 10(b). When the external force is applied, the ZMP_y departs from the ZMP stability region and triggers Step 2. Step 2 is complete in Fig. 10(c), and Step 3 begins. It is clear that the ZMP control in Step 2 counteracts the external force, as shown in Fig. 10(c) (an external force of +0.4 N is applied from left to right). Step 3(the contracting of the stance leg(right leg)) is completed as shown in Fig. 10 (d). Because the swing leg(left leg) is at a relatively lower position in Fig. 10(c), there is no need to move the swing leg to a lower position by using the foot-tip Jacobian based constrained optimization.

The gaits of the simulation results for Cases 4, 5, and 6 are also described in Fig. 11. Cases 4, 5, and 6 represent almost identical gaits. Figure 11(a)–(c) are from a sagittal plane view, and Fig. 11(d) and (e) are from a lateral plane view. The initial posture is described in Fig. 11(a). The left leg is set behind as the swing leg, and the right leg is the stance leg. The external force is applied at one quarter of a stride as shown in Fig. 11(b), and eventually, ZMP_y depart from the ZMP stability region and triggers Step 2 as shown in Fig. 11(c). Step 2 is performed and results in a gait as shown in Fig. 11(d)

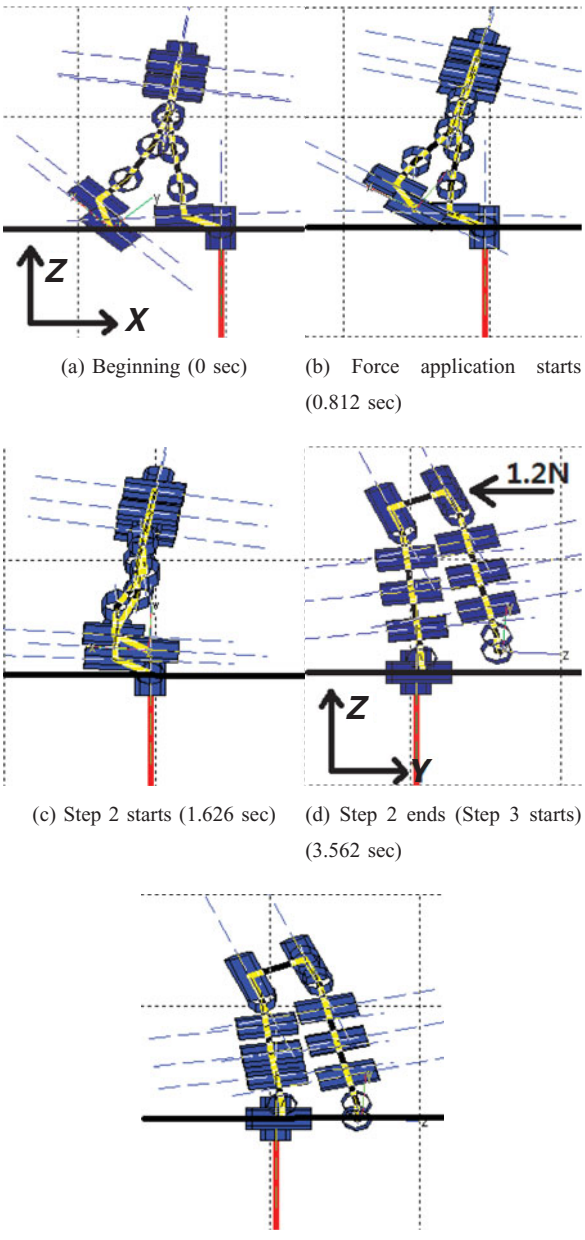

(a) Beginning (0 sec) (b) Force application starts (0.812 sec)

(c) Step 2 starts (1.626 sec) (d) Step 2 ends (Step 3 starts) (3.562 sec)

(e) Step 3 ends (4.562 sec)

Fig. 11. Balancing pictures of LRH-1 (Case 4, 5, 6). (a) Beginning (0 s). (b) Force application starts (0.812 s). (c) Step 2 starts (1.626 s). (d) Step 2 ends (Step 3 starts) (3.562 s). (e) Step 3 ends (4.562 s).

and triggers Step 3. Step 3 simply contracts the stance leg and ends as shown in Fig. 11(e), where no foot-tip Jacobian based constrained optimization is required because at the end of Step 2, the swing leg is in a sufficiently low position.

The overall time of the gait control strategy is 4.904 s for Cases 1, 2 and 3 and 4.562 s for Cases 4, 5 and 6. The Step 2 control time is longer in Cases 1, 2 and 3 relative to Cases 4, 5 and 6, which leads to the overall time differences between Cases 1, 2 and 3 and Cases 4, 5 and 6.

5.2. The ZMP results

The ZMP results of the simulation in cases 1, 2, and 3 are described in Fig. 12. In the simulation, the upper limit and the lower limit of the x-direction ZMP are 0 m and -0.1 m, respectively, and the upper limit and the lower limit of the y-direction ZMP are +0.03 m and -0.03 m, respectively. The upper picture in Fig. 12 represents the ZMP_x graphs and the lower picture represents the ZMP_y

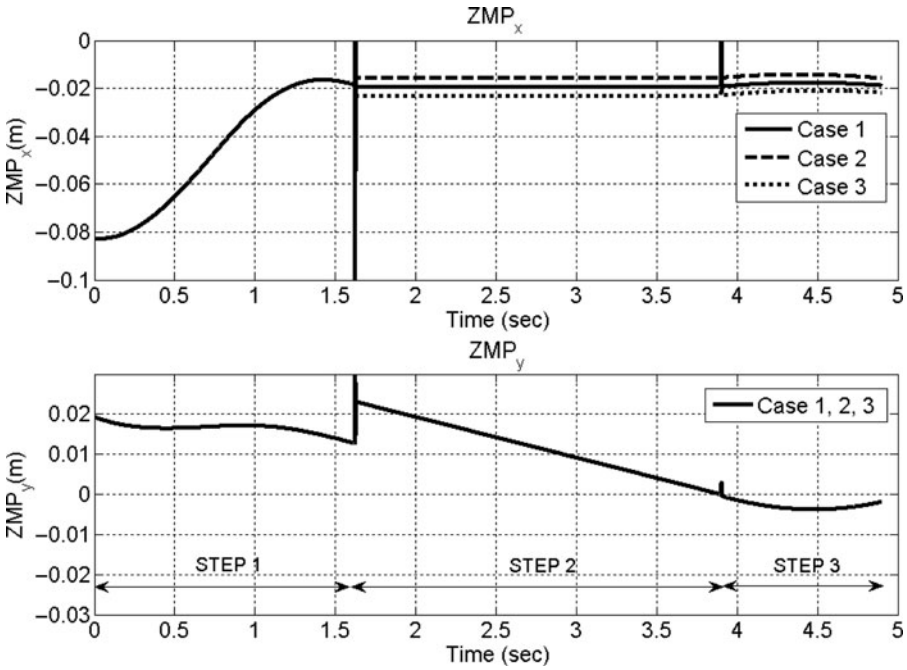

Fig. 12. ZMP graphs of simulation results (Case 1, 2, 3).

graph in which Case 1, 2 and 3 are identical. Step 1, 2 and 3 control regions are expressed using double-arrowed lines. The ±0.05N perturbation force in the X direction results in ZMP_x shifts as shown in Fig. 12. The ZMP_y graph abruptly changes at the end of the Step 1 because the +0.4 N external force is applied to the biped robot. The Step 2 control strategy nearly linearly controls the ZMP_y until 0 is reached. Contracting the stance leg in Step 3 slightly modifies the ZMP_y value.

The ZMP results of the simulation in cases 4, 5, and 6 are described in Fig. 13. In all three cases, the ZMP_y characteristic is identical. The ±0.05 N perturbation force in the X direction results in ZMP_x shifts as shown in Fig. 13. The ZMP_x graph in the Step 2 and 3 regions is nearly flat because the Step 2 and 3 control strategies have insignificant effects on ZMP_x. The −1.2 N external force application at approximately 0.812 s results in an abrupt change of ZMP_y, and ZMP_y departs the ZMP stability region at 1.626 s. Step 2 linearly controls the ZMP_y value until a value of 0 is reached. Contracting the stance leg in Step 3 just perturbs the ZMP_y value.

5.3. The torque results

The right (stance) leg joint actuating torques in Cases 1 and 4 are described in Figs. 14 and 15, respectively. Each of the three graphs in Figs. 14 and 15 represents the roll direction ankle, pitch direction knee and roll direction hip joint actuating torques of the stance leg. The roll direction ankle torque graphs in Figs. 14 and 15 represent nearly identical characteristics as the ZMP_y graphs in Figs. 12 and 13 because the roll direction ankle torque directly affects ZMP_y. The ankle torque range is $-0.2 \sim 0.2$ Nm in Case 1 and $-0.3 \sim 0.1$ Nm in Case 4. The pitch direction knee torque graphs in Figs. 14 and 15 are nearly flat in Step 2 but increase linearly in Step 3 because contracting the stance leg in Step 3 increases the knee torque demands. The roll direction hip torque is nearly flat in every ranges as shown in Figs. 14 and 15 and its value is approximately −0.5 Nm.

6. The Experimental Results

In this section, the experimental results are shown. The experiment is divided into two parts. First, the external force is applied in the $+Y$ direction(Case 1 in Table III). Second, the external force is applied in the $-Y$ direction(Case 4 in Table III). We performed the experiments for these two cases because the results can be used to verify the proposed control strategy clearly. We applied this force

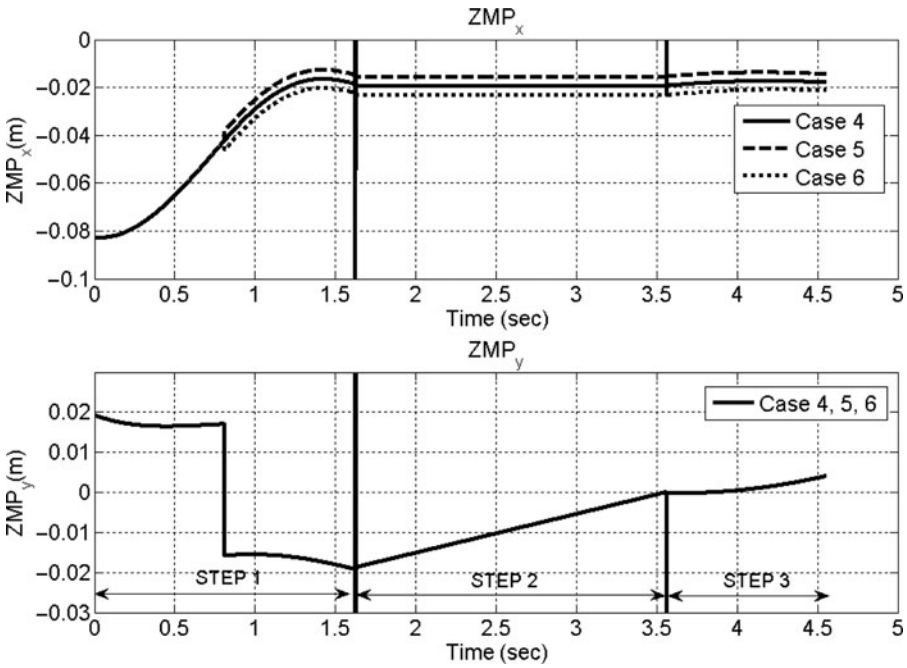

Fig. 13. ZMP graphs of simulation results (Case 4, 5, 6).

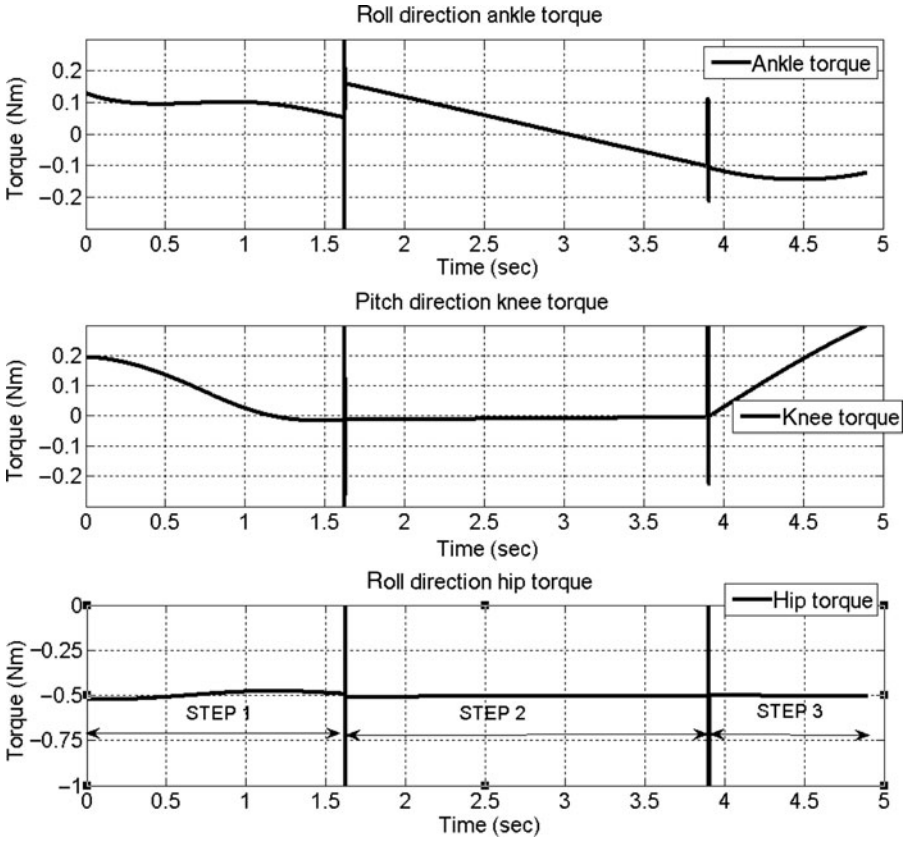

Fig. 14. Actuating torque graphs of right (stance) leg (Case 1).

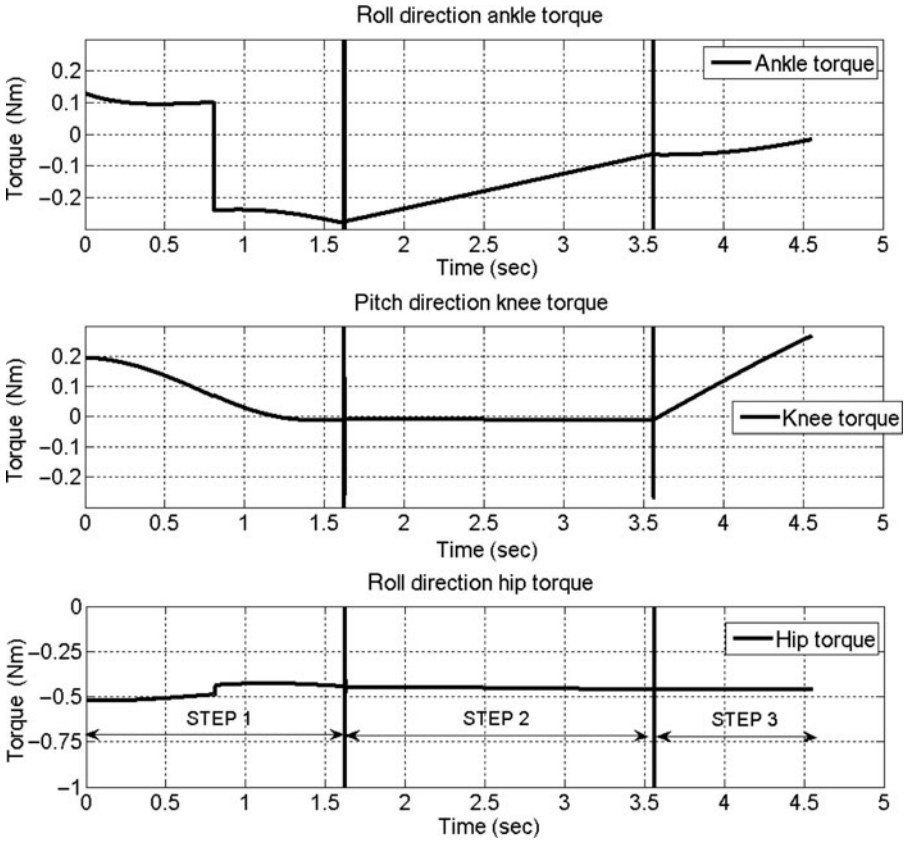

Fig. 15. Actuating torque graphs of right (stance) leg (Case 4).

by pushing the pelvis of LRH-1 using a finger. The exact magnitude of the force was not measured. For future studies, we plan to measure the magnitude of the externally applied force.

6.1. The gaits characteristics

In this subsection, we represent the gait characteristics of the biped robot. The pictures of the first experiment, where the external force is applied in the $+Y$ direction are provided in Fig. 16. The pictures are taken in front of the robot. Figure 16(a) represents the initial position of LRH-1. The robot is about to move. As it walks, a force in the $+Y$ direction is applied to the pelvis of LRH-1 using a finger as shown in Fig. 16(b). After detecting this abnormal situation by measuring the ZMP, the force-resisting balance control strategy is applied in Fig. 16(c). Figure 16(d) represents the final double support phase state after completing all the force-resisting control strategies. Figure 16(b) and (c) appear to be identical because the overall time of step 2 of the force resisting control strategy is small. In other words, the Y direction ZMP of the stance leg became zero in a relatively small time interval. The detailed ZMP results are provided in the subsequent chapter.

The figure corresponding to the second experiment, where an external force in the $-Y$ direction is applied is given in Fig. 17. Figure 17(a) represents the initial position of LRH-1. The force in the $-Y$ direction is applied to the pelvis of LRH-1 using a finger, as shown in Fig. 17(b). Step 2 of the force-resisting balance control strategy is applied in Fig. 17(c). The robot counteracts the externally applied force. Figure 17(d) represents the final double support phase state.

6.2. The ZMP results

The ZMP results of the first and second experiments are represented in this section. The system of coordinates of the ZMP is in accordance with that of Fig. 4. The ZMP result of the first experiment(Case 1 in Table III) is represented in Fig. 18 and that of the second experiment(Case 4 in Table III) is represented in Fig. 19. The top graph in Fig. 18 represents the x-direction ZMP and the lower graph in Fig. 18 depicts the y-direction ZMP. The upper limit and the lower limit of the

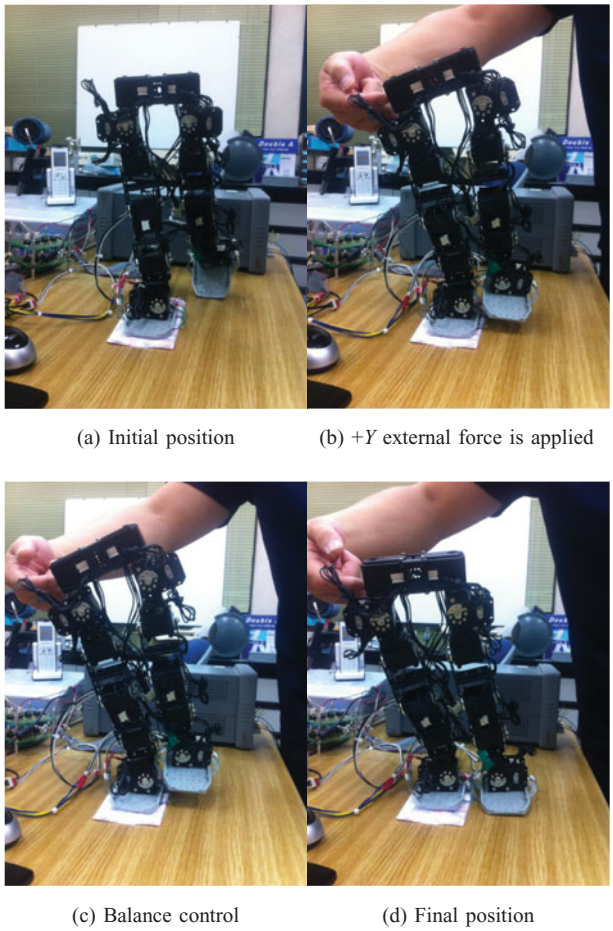

(a) Initial position (b) $+Y$ external force is applied

(c) Balance control (d) Final position

Fig. 16. Force-resisting balance control strategy in $+Y$ external force. (a) Initial position. (b) $+Y$ external force is applied. (c) Balance control. (d) Final position.

x-direction ZMP are -0.025 m and -0.075 m, respectively. The upper limit is not zero because the ZMP is measured by an force sensing resistor (FSR) which measures the force over a large area. The upper limit and the lower limit of the y-direction ZMP are +0.025 m and -0.025 m, respectively. In the simulation, the upper limit and the lower limit of x-direction ZMP are 0 m and -0.1 m and the upper limit and the lower limit of the y-direction ZMP are +0.03 m and -0.03 m, respectively, as stated previously.

The x-direction ZMP results of both experiments are almost identical because there is only an external force disturbance in the $\pm Y$ direction. Until approximately 4 s, the X-direction ZMP is approximately -0.025 m and afterward, the ZMP becomes -0.075 m which means that the X-direction ZMP moves from the front side to the back side of the sole. This phenomenon occurs because the gait causes the center of pressure to move from the front to the back.

If we look at the y-direction ZMP of the first experiment in Fig. 18, an important feature can be seen at approximately 4.5 s. At this time, the external force in the $+Y$ direction is applied and the ZMP value is approximately +0.025 m. 0.4 s later, the LRH-2 detects the abnormal situation, and performs the force-resisting balance control strategy. At approximately 5.4 s. the Y-direction ZMP becomes zero. This halts the strategy and triggers Step 3. The overall control strategy concludes at approximately 7.2 s.

In the y-direction ZMP of the second experiment in Fig. 19, the $-Y$ direction force is applied at 4.2 s and the ZMP reaches a peak value of -0.025 m at approximately 5.5 s. LRH-1 detects the abnormal situation at this time using the ZMP and performs step 2 of the force-resisting balance control strategy. The strategy concludes at 7.2 s when the ZMP reaches zero. Afterward, LRH-1 progresses from the SSP to the DSP by Step 3. The overall control strategy concludes at approximately 8.6 s.

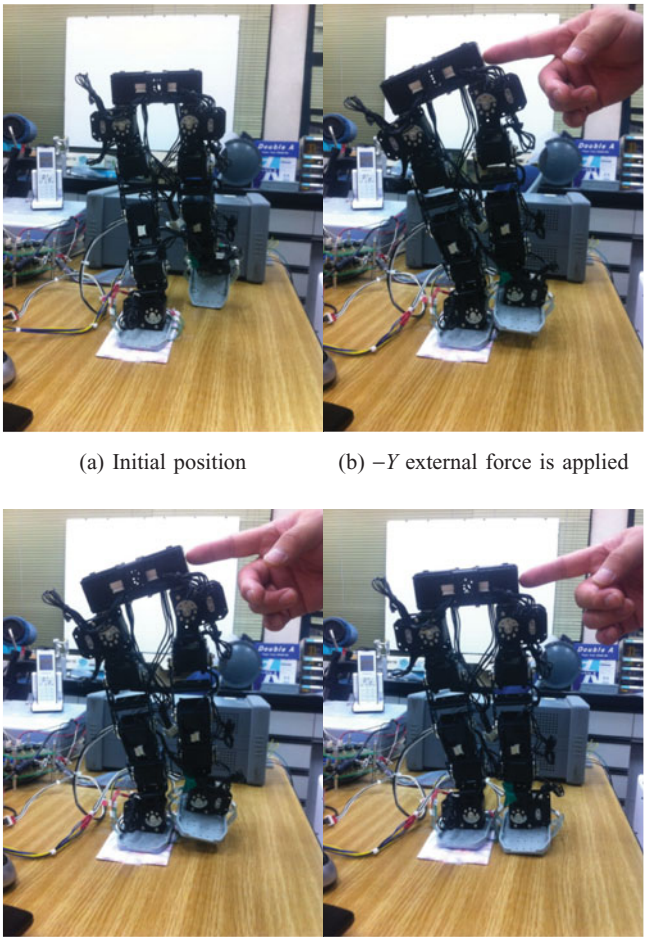

(a) Initial position (b) $-Y$ external force is applied

(c) Balance control (d) Final position

Fig. 17. Force-resisting balance control strategy in $-Y$ external force. (a) Initial position. (b) $-Y$ external force is applied. (c) Balance control. (d) Final position.

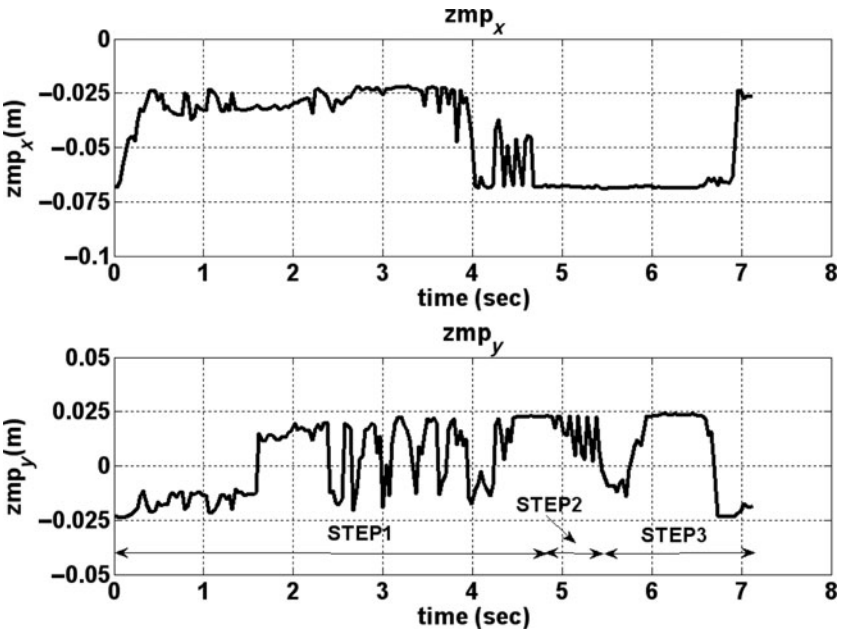

Fig. 18. ZMP graphs of stance foot(+Y direction external force).

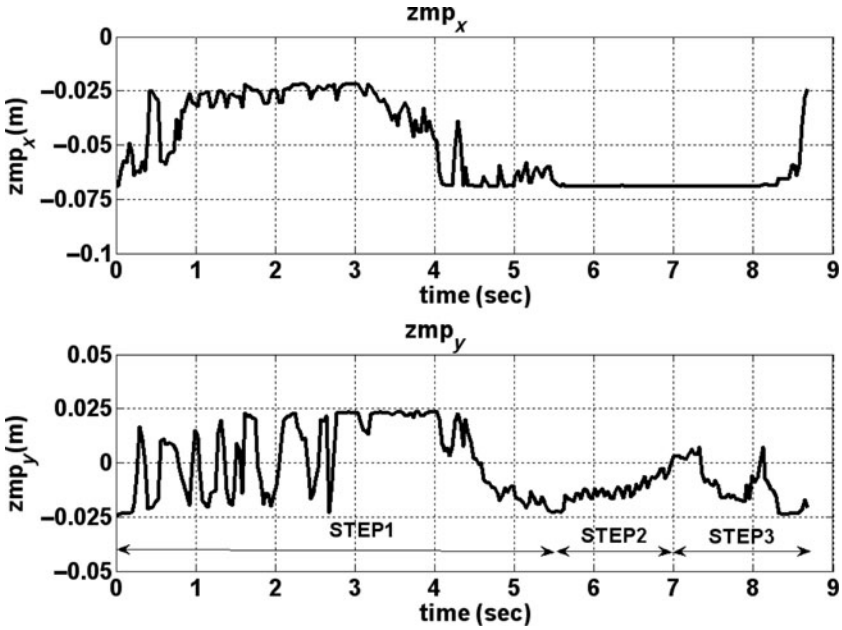

Fig. 19. ZMP graphs of stance foot($-Y$ direction external force).

6.3. Comparison of the ZMP results between simulations and experiments

In this subsection, the ZMP results are compared between the simulations and the experiments. As previously mentioned, the walking gait in the experiment is different from that in the simulation because the walking gait is tuned during experiment.

We can compare Fig. 12 with Fig. 18 and Fig. 13 with Fig. 19. The ZMP_x graphs in Step 2 and Step 3 in the four figures are nearly flat, which means that during Step 2 and Step 3, ZMP_x has an insignificant influences on both in the experiments and the simulations. However, the absolute value is different from the simulations and the experiments. In the simulations, the ZMP_x value is approximately -0.02 m, while in the experiments, it is approximately -0.075 m, which means that the center of pressure is located at the front of the sole in the simulation and the rear of the sole in the experiment.

The ZMP_y graphs for Step 2 in the simulations are nearly linear until a value of zero is reached, while in the experiment, it appears to be complex. In Fig. 18, the ZMP_y graph in Step 2 has a zig-zag shape and eventually becomes zero. This zig-zag shape is a result of the robot being pushed by a finger. Actually, a constant pushing force cannot be maintained and will fluctuate, which results in the zig-zag shape. However, the ZMP_y value becomes zero using the Step 2 control. In Fig. 19, the ZMP_y graph in Step 2 is linear with minor fluctuation, which is in good agreement with the simulation.

7. Conclusion

In this paper, we proposed a force-resisting balance control strategy for a walking biped robot subject to a sudden, unknown, continuous external force. First, we discussed the motivation behind this research, and explained why the suggested strategy is needed. Second, we explained the suggested force balance control strategy using steps 1, 2, and 3. This control strategy uses the discretized inverted pendulum model, the COG Jacobian, the foottip Jacobian and linear quadratic programming technique. Third, we verified the suggested control strategy using numerical simulations. The simulations using the biped robot LHR-1 model were performed in all six cases, and the resulting gait trajectory, ZMP profile and joint torque profile were explained. Fourth, experiments using the biped robot LHR-1 were performed. The experiments were performed in two cases, and the gait characteristics and the ZMP trajectory results were investigated. The numerical simulations and the experimental results were compared, and they verified the proposed control strategy. Future research will involves an improved

control strategy, that makes use of a more elaborate objective function and a fuzzy or neural network to solve these strategies in real time.

Acknowledgement
This work was supported by the Industrial Strategic technology development program, 10045252, "Development of Robot task intelligence technology that can perform task more than 80% in inexperience situation through autonomous knowledge acquisition and adaptational knowledge application" funded By the Ministry of Trade, industry and Energy (MI, Korea)

References

1. M. Vukobratovic and B. Borovac, "Zero moment point: Thirty five years of its life," *Int. J. Humanoid Robot* **1**(1), 157–173 (2004).
2. T. McGeer, "Passive dynamic walking," *Int. J. Robot. Res.* **9**(2), 62–82 (1990).
3. T. Geng and J. Q. Gan, "Planar biped walking with an equilibrium point controller and state machines," *IEEE/ASME Trans. Mechatronics* **15**(2), 253–260 (2010).
4. F. J. Berenguer and F. M. Monasterio-Huelin, "Zappa, a quasi-passive biped walking robot with a tail: Modeling, behavior, and kinematic estimation using accelerometers," *IEEE Trans. Indust. Electron.* **55**(9), 3281–3289 (2010).
5. T. Sato, S. Sakaino and K. Ohnishi, "Real-time walking trajectory generation method with three-mass models at constant body height for three-dimensional biped robots," *IEEE Trans. Indust. Electron.* **58**(2), 376–383 (2011).
6. D. Goswami and P. Vadakkepat, "Planar bipedal jumping gaits with stable landing," *IEEE Trans. Robot.* **25**(5), 1030–1046 (2009).
7. S. Kajita, T. Nagasaki, K. Kaneko and H. Hirukawa, "ZMP-based biped running control," *IEEE Robot. Autom. Mag.* **14**(2), 63–72 (2007).
8. Q. Huang *et al.*, "Balance Control of a Biped Robot Combining Off-line Pattern with Real-time Modification," *Proceedings of the 2000 IEEE International Conference on Robotics and Automation* (2000) pp. 3346–3352.
9. H. Hemani and P. Camana, "Nonlinear feedback in simple locomotion systems," *IEEE Trans. Autom. Control* **21**(6), 855–860 (1976).
10. F. Horak and L. Nashner, "Central programming of postural movements: Adaptation to altered support-surface configurations," *J. Neurophysiol.* **55**(6), 1369–1381 (1986).
11. D. N. Nenchev and A. Nishio, "Ankle and hip strategies for balance recovery of a biped subjected to an impact," *Robotica* **26**(5), 643–653 (2008).
12. B. Stephens, "Integral Control of Humanoid Balance," *Proceedings of the IEEE/RSJ International Conference on Intelligent Robots and Systems (IROS)* (2007) pp. 4020–4027.
13. R. Goddard, H. Hemami and F. Weimer, "Biped side step in the frontal plane," *IEEE Trans. Autom. Control* **28**(2), 179–187 (1983).
14. D. Winter, "Human balance and posture control during standing and walking," *Gait Posture* **3**(4), 193–214 (1995).
15. X. Deng-Peng and L. Xu, "Multiple balance strategies for humanoid standing control," *Acta Autom. Sin.* **37**(2), 228–233 (2011).
16. B. Stephens, "Humanoid Push Recovery," *Proceedings of the 7th IEEE-RAS International Conference on Humanoid Robots* (2007) pp. 589–595.
17. J. E. Pratt, J. Carff, S. Drakunov and A. Goswami, "Capture Point: A Step Toward Humanoid Push Recovery," *Proceedings of the IEEE-RAS International Conference on Humanoid Robots* (2006) pp. 200–207.
18. N. Motoi, M. Ikebe and K. Ohnishi, "Real-time gait planning for pushing motion of humanoid robot," *IEEE Trans. Indust. Inform.* **3**(2), 154–163 (2007).
19. K. Harada, S. Kajita, F. Kanehiro, K. Fujiwara, K. Kaneko, K. Yokoi and H. Hirukawa, "Walking motion for pushing manipulation by a humanoid robot," *J. Robot. Soc. Japan.* **22**(3), 392–399 (2004).
20. T. Komura, H. Leung, S. Kudoh and J. Kuffner, "A Feedback Controller for Biped Humanoids that can Counteract Large Perturbation during Gait," *Proceedings of the 2005 IEEE International Conference Robotics and Automation (ICRA)* (2005) pp. 1989–1995.
21. A. Yasin, Q. Huang, Q. Xu and W. Ahang, "Biped Robot Push Detection and Recovery," *Proceedings of the IEEE International Conference on Information and Automation* (2012) pp. 993–998.
22. S. J. Yi, B. T. Zhang, D. Hong and D. D. Lee, "Learning Full Body Push Recovery Control for Small Humanoid Robots," *Proceedings of the IEEE International Conference on Robotics and Automation* (2011) pp. 2047–2052.
23. S. J. Yi, B. T. Zhang, D. Hong and D. D. Lee, "Online Learning of a Full Body Push Recovery Controller for Omnidirectional Walking," *Proceedings of the 11th IEEE-RAS International Conference on Humanoid Robots* (2011) pp. 1–6.

24. T. S. Li, Y. T. Su, S. H. Liu, J. J. Hu and C. C. Chen, "Dynamic balance control for biped robot walking using sensor fusion, Kalman Filter, and Fuzzy logic," *IEEE Trans. Indust. Electron.* **59**(11), 4394–4408 (2012).
25. Y. J. Kim, J. Y. Lee and J. J. Lee, "A Balance Control Strategy of A Walking Biped Robot in An Externally Applied Force," *Proceeding of the IEEE International Conference on Information and Automation* (2012) pp. 572–577.
26. K. Demura, "practice! easy! robot simulation," *Morikita 2007*.
27. Y. J. Kim, J. Y. Lee and J. J. Lee, "Bipedal Walking Trajectory Generation Using Tchebychev Method," *Proceedings of the International Conference on Mechatronics and Informatics* (2011) pp. 34–42.
28. S. Kajita, F. Kanehiko, K. Kaneko, K. Yokoi and H. Hirukawa, "The 3D Linear Inverted Pendulum Mode: A Simple Modeling for a Biped Walking Pattern Generation," *Proceedings of the IEEE/RSJ International Conference on Intelligent Robots and Systems* (2001) pp. 239–246.
29. T. Sugihara and Y. Nakamura, "Whole-body Cooperative Balancing of Humanoid Robot Using COG Jacobian," *Proceedings of the 2002 IEEE/RSJ International Conference on Intelligent Robots and Systems* (2002) pp. 2575–2580.